Available online at www.sciencedirect.com

SciVerse ScienceDirect

Ceramics International 38 (2012) 5535–5541

CERAMICS INTERNATIONAL

www.elsevier.com/locate/ceramint

Sol–gel synthesis of $La_{0.6}Sr_{0.4}CoO_{3-x}$ and $Sm_{0.5}Sr_{0.5}CoO_{3-x}$ cathode nanopowders for solid oxide fuel cells

Narottam P. Bansal *, Brent Wise

National Aeronautics and Space Administration, Glenn Research Center, Cleveland, OH 44135, USA

Received 14 February 2012; received in revised form 27 March 2012; accepted 28 March 2012
Available online 4 April 2012

Abstract

Nano-powders of $La_{0.6}Sr_{0.4}CoO_{3-x}$ (LSC) and $Sm_{0.5}Sr_{0.5}CoO_{3-x}$ (SSC) compositions, which are being investigated as cathode materials for intermediate temperature solid oxide fuel cells (IT-SOFCs) with $La(Sr)Ga(Mg)O_{3-x}$ (LSGM) as the electrolyte, were synthesized by low-temperature sol–gel method using metal nitrates and citric acid. Thermal decomposition of the citrate gels was followed by simultaneous DSC/TGA methods. Development of phases in the gels, on heat treatments at various temperatures, was monitored by X-ray diffraction. Sol–gel powders calcined at 550–1000 °C consisted of a number of phases. Single perovskite phase $La_{0.6}Sr_{0.4}CoO_{3-x}$ or $Sm_{0.5}Sr_{0.5}CoO_{3-x}$ powders were obtained at 1200 °C and 1300 °C, respectively. Morphological analysis of the powders calcined at various temperatures was done by scanning electron microscopy. The average crystallite size of the powders was ~15 nm after 700 °C calcinations and slowly increased to 70–100 nm after heat treatments at 1300–1400 °C.
Published by Elsevier Ltd and Techna Group S.r.l.

Keywords: D. Perovskites; Solid oxide fuel cell; Cathodes; Nanopowders

1. Introduction

A fuel cell is an electrochemical device which continuously converts chemical energy of a fuel directly into electrical energy. A fuel cell consists of an electrolyte, an anode and a cathode. Various types of fuel cells are available such as direct methanol fuel cell, alkaline fuel cell, proton exchange membrane fuel cell, phosphoric acid fuel cell, molten carbonate fuel cell, and solid oxide fuel cell (SOFC). The salient features of SOFC are all solid construction, high-temperature electrochemical reaction based operation, resulting in clean and efficient power generation from a variety of fuels. Solid oxide fuel cells [1] are being developed for a broad range of applications such as in portable electronic devices, automobiles, power generation, auxiliary power units and electric propulsion in aeronautics.

Doped lanthanum cobaltites $La_{1-x}Sr_xCoO_{3-y}$ and samarium cobaltites $Sm_{1-x}Sr_xCoO_{3-y}$ show mixed ionic-electronic conduction and high catalytic reactivities for oxygen reduction. For example, the electronic conductivity of $La_{1-x}Sr_xCoO_{3-y}$ is greater than 1000 S/cm at 800 °C, while the ionic conductivity is between 0.1 and 1 S/cm [3]. Among others, $La_{0.6}Sr_{0.4}CoO_{3-x}$ (LSC) and $Sm_{0.5}Sr_{0.5}CoO_{3-x}$ (SSC) perovskites have attracted attention as cathode materials for intermediate temperature SOFC with $La(Sr)Ga(Mg)O_{3-y}$ (LSGM) electrolyte. LSC is also used in a number of other applications such as gas sensors, oxygen catalyst, and ferroelectric random access memories. High purity $Sm_{1-x}Sr_xCoO_{3-y}$ and $La_{0.6}Sr_{0.4}CoO_{3-x}$ powders are needed for various applications. A number of chemical approaches such as, solid state calcination, combustion synthesis [4], ultrasonic spray pyrolysis [5], sol–gel [2,6,7], freeze drying, co-precipitation, hydrothermal, etc. have been generally utilized for ceramic powder processing.

The primary objective of this study was the synthesis of $Sm_{1-x}Sr_xCoO_{3-y}$ and $La_{0.6}Sr_{0.4}CoO_{3-x}$ perovskite nanopowders by the low-temperature citric acid sol–gel approach. Thermal decomposition behavior of the gel was investigated by DSC–TGA method. Development of crystalline phases on heat treatments of the gel at various temperatures was followed by X-ray diffraction. Morphology of the powders was also characterized by scanning electron microscopy (SEM).

* Corresponding author. Tel.: +1 216 433 3855; fax: +1 216 433 5544.
E-mail address: Narottam.P.Bansal@nasa.gov (N.P. Bansal).

0272-8842/$36.00. Published by Elsevier Ltd and Techna Group S.r.l.
http://dx.doi.org/10.1016/j.ceramint.2012.03.069

2. Experimental methods

2.1. Powder synthesis

The starting materials used in the synthesis were reagent grade metal nitrates $Sm(NO_3)_3{\cdot}6H_2O$, $Sr(NO_3)_2$, $Co(NO_3)_2{\cdot}6H_2O$, $La(NO_3)_3{\cdot}6H_2O$ and citric acid $C_6H_8O_7{\cdot}H_2O$ from Alfa Aesar. A flow chart showing the various steps involved in the synthesis of powders by the sol–gel process is shown in Fig. 1. Appropriate quantities of the metal nitrates, to yield 100 g of the final SSC or LSC oxide powder, were dissolved in deionized water. Calculated amount of citric acid, 1.5 moles per mole of metal nitrate, was also dissolved in deionized water. The citric acid solution was slowly added to the metal nitrate aqueous solution under constant stirring. The resulting clear and transparent red colored solution was heated at 80 °C for several hours. The solution became increasingly viscous due to polymerization reaction and slowly changed to resin like consistency. Dark brown nitrous oxide fumes were also formed from the decomposition of nitric acid which was produced by the reaction of metal nitrates with citric acid. The gel was calcined at 300 °C for ∼15 h when it converted into black powder. No change was apparent in the gel after further heat treatment at 550 °C for 20 h in air. Small portions (∼1 g) of this powder were heat treated in air at various temperatures between 700 and 1500 °C for 1 h to study the development of crystalline phases.

2.2. Characterization

Simultaneous differential scanning calorimetry and thermal gravimetric analysis (DSC–TGA) of the gel were carried out using Netzsch STA 409C system which was interfaced with computerized data acquisition and analysis system at a scan rate of 10 °C/min in air. Powder X-ray diffraction (XRD) patterns were recorded at room temperature using a step scan procedure (0.02°/2θ step, time per step 0.5 or 1 s) in the 2θ range 10–70° on a Philips ADP-3600 automated diffractometer equipped with a crystal monochromator employing copper K_α radiation. Microstructural analysis was carried out using a JEOL JSM-840A scanning electron microscope (SEM). Prior to analysis, a thin layer of Pt or carbon was evaporated onto the SEM specimens for electrical conductivity.

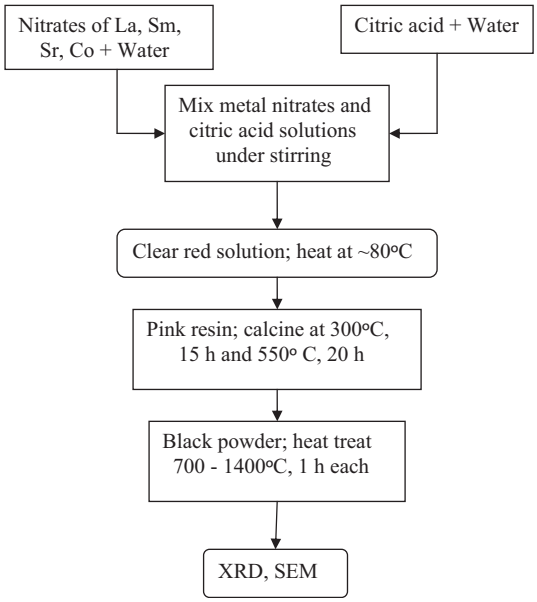

Fig. 1. Flow chart for sol–gel synthesis of $Sm_{0.5}Sr_{0.5}CoO_{3-x}$ and $La_{0.6}Sr_{0.4}CoO_{3-x}$ nanopowders.

3. Results and discussion

3.1. Thermal analyses of gels

Fig. 2 shows the DSC/TGA curves recorded at a heating rate of 10 °C/min in air from room temperature to 1200 °C for the pink SSC resin obtained during sol–gel synthesis. Similar results were obtained for the LSC composition and will not be reported here. A small endothermic peak at ∼115 °C is present in DTA which is accompanied by a small weight loss of ∼2% due to the evaporation of residual absorbed and hydrated water. Between 130 °C and ∼375 °C, several strong exothermic peaks are present in the DTA. Each exothermic event is accompanied by weight loss step in the TGA. These exothermic events are probably associated with the combustion and/or oxidative decomposition of the various metal citrate chelates, excess citric acid and other organic residuals. The small exotherm at ∼475 °C is probably due to the crystallization of the complex oxide $SmCoO_3$ through the reaction of samarium and cobalt oxides formed from the decomposition of metal chelates. This is supported by the fact that this exotherm is not accompanied by any weight loss event in the TGA. On heat treatment, strontium citrate chelate is first converted into $SrCO_3$. Part of this $SrCO_3$ reacts with samarium and cobalt oxides to form complex metal oxide phases. The unreacted residual $SrCO_3$ decomposes into SrO at higher temperatures as indicated by a small endothermic peak at ∼900 °C in DTA. The total loss of sample weight up to 1200 °C is 73%.

3.2. Phase formation and microstructure analysis

X-ray diffraction patterns of LSC and SSC gels after thermal treatments at various temperatures from 550 to 1400 °C are

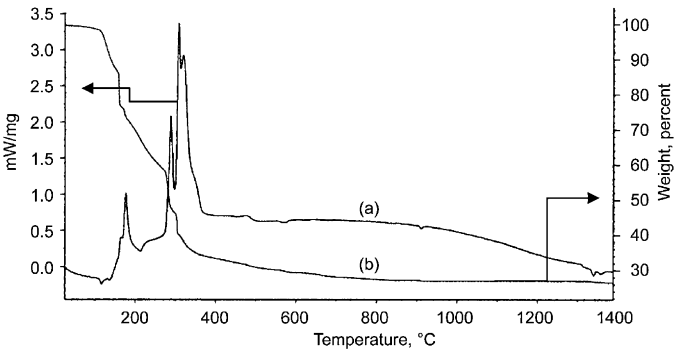

Fig. 2. (a) DSC and (b) TGA curves of $Sm_{0.5}Sr_{0.5}CoO_{3-x}$ gel recorded at the heating rate of 10 °C/min in air.

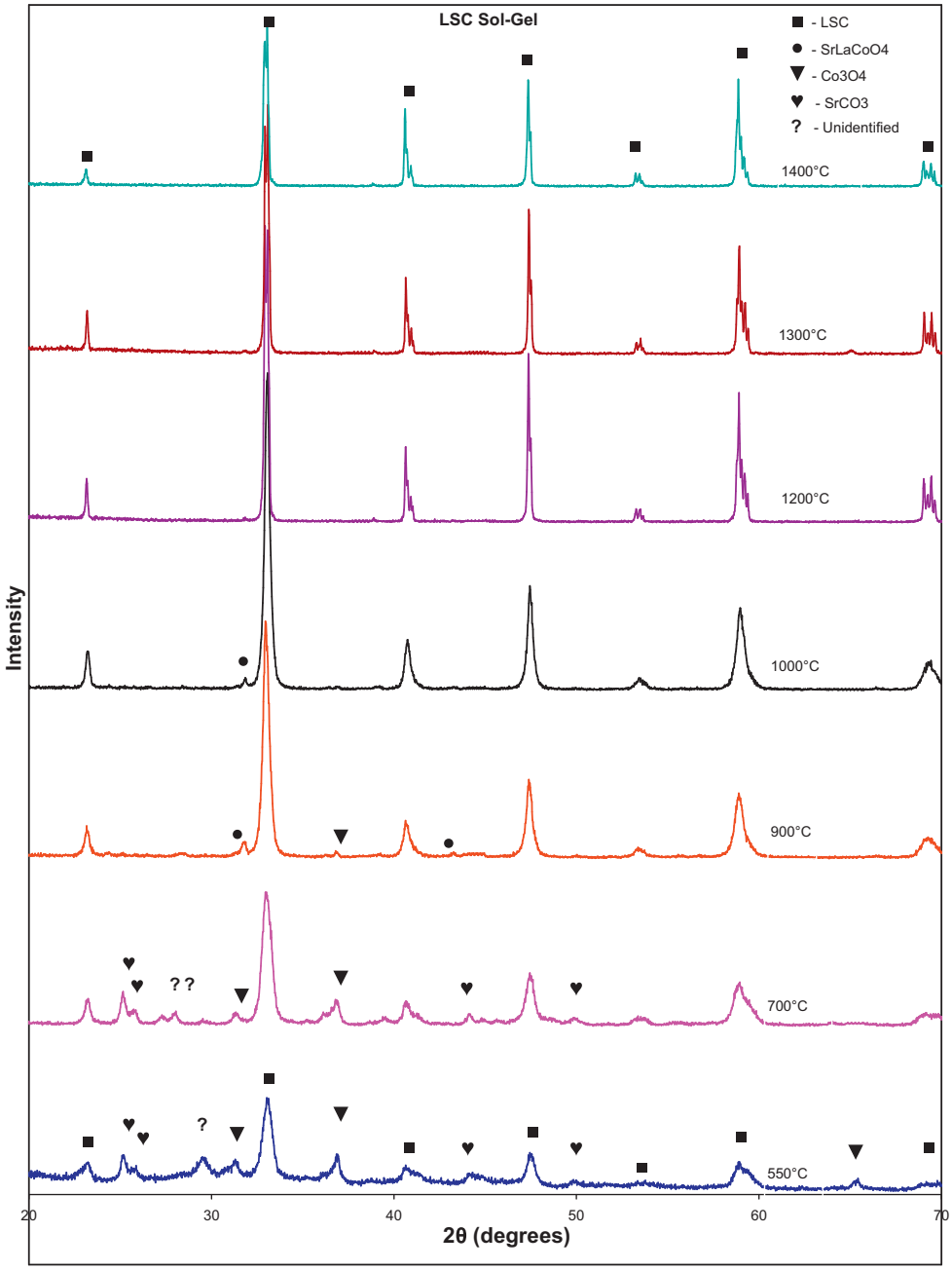

Fig. 3. X-ray diffraction patterns of $La_{0.6}Sr_{0.4}CoO_{3-x}$ sol–gel nanopowders calcined at various temperatures.

shown in Figs. 3 and 4, respectively. The results for the development of crystalline phases as a function of heat treatments are summarized in Table 1. After calcination at 550 °C, the pink LSC resin decomposed into $La_{0.6}Sr_{0.4}CoO_{3-x}$, Co_3O_4, $SrCO_3$ whereas Co_3O_4, $SmCoO_3$, and $SrCO_3$ were formed in the SSC system. Small unknown peaks were also present in both systems. After heating at 700 °C, no additional phase was observed in the LSC system, whereas $Sm_{0.5}Sr_{0.5}CoO_{3-x}$, $SrCO_3$, and Co_3O_4 phases were detected in the SSC system. On heat treatment at 900 °C, $SrCO_3$ which was formed at lower temperatures, decomposed to SrO and reacted with other oxides to form $SrLaCoO_4$ or $Sr_3Co_2O_6$. The phases present after 1000 °C treatment were $La_{0.6}Sr_{0.4}CoO_{3-x}$ and $SrLaCoO_4$ in LSC system and $Sm_{0.5}Sr_{0.5}CoO_{3-x}$, $Sr_3Co_2O_6$, Co_3O_4 in the SSC system. On heat treatment at 1200 °C, only perovskite phase-pure $La_{0.6}Sr_{0.4}CoO_{3-x}$ was detected in the LSC system whereas the SSC system still consisted of $Sm_{0.5}Sr_{0.5}CoO_{3-x}$ and $Sr_3Co_2O_6$. The SSC powder converted to perovskite phase-pure $Sm_{0.5}Sr_{0.5}CoO_{3-x}$ only after heat treatment at 1300 °C.

After each thermal treatment, the average crystallite size was evaluated from X-ray line broadening using the Scherrer formula [8]:

$$t = \frac{0.9\lambda}{B\cos\theta_B} \quad (1)$$

where t is the average crystallite size, λ is the wave length of copper K_α radiation, B is the width (in radian) of the XRD

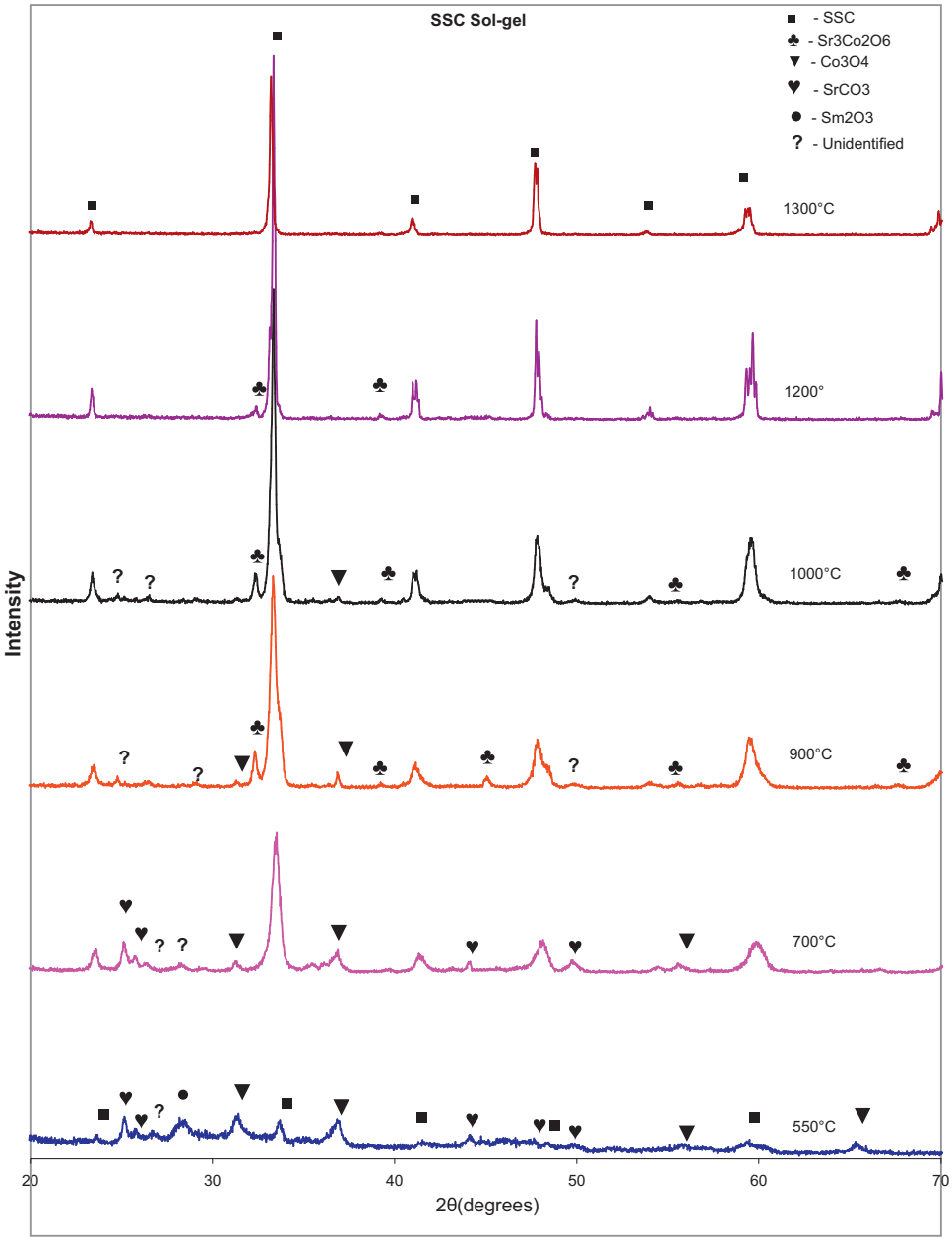

Fig. 4. X-ray diffraction patterns of $Sm_{0.5}Sr_{0.5}CoO_{3-x}$ sol–gel nanopowders calcined at various temperatures.

diffraction peak at half its maximum intensity, and θ_B is the Bragg diffraction angle of the line. Correction for the line broadening by the instrument was applied utilizing a large particle size silicon standard and the equation:

$$B^2 = B_M^2 - B_S^2 \quad (2)$$

where B_M and B_S are the measured widths, at half maximum intensity, of the lines from the sample and the standard, respectively. Values of average grain sizes of the as synthesized SSC and LSC powders and of those after heat treatments at various temperatures are summarized in Table 1. The average crystallite size of the powders was ~15 nm after 700 °C calcinations and slowly increased to 70–100 nm after heat treatments at 1300–1400 °C. The X-ray line broadening method can be used only for the size determination of small crystallites (~100 nm). Besides, the values obtained are not the real particle size, but the average size of coherently diffracting domains; the latter being usually much smaller than the actual size of the particles. The average crystallite size of the LSC nanopowder synthesized by the Pechini method was reported [7] to be about 18 nm which is similar to that observed in the current study. The size of both SSC and LSC powders obtained in the present study is also similar to those processed earlier by the solution combustion synthesis method [4].

The SEM micrographs of $La_{0.6}Sr_{0.4}CoO_{3-x}$ and $Sm_{0.5}Sr_{0.5}CoO_{3-x}$ powders prepared by sol–gel synthesis after thermal treatments at 550 °C for 20 h, 1000 °C for 1 h, and 1200 °C for 1 h in air are shown in Figs. 5 and 6, respectively. The as-synthesized powders as well as those after heat

Table 1
X-ray diffraction analysis of $Sm_{0.5}Sr_{0.5}CoO_{3-x}$ and $La_{0.6}Sr_{0.4}CoO_{3-x}$ sol–gel nanopowders after various heat treatments.

System	Heat treatment		Crystalline phases[a]	Average crystallite size (nm)[b]
	Temp. (°C)	Time (h)		
$La_{0.6}Sr_{0.4}CoO_{3-x}$	550	20	$La_{0.6}Sr_{0.4}CoO_{3-x}$, Co_3O_4, $SrCO_3$, unknown peak at $d = 0.318$ nm and few other small peaks	–
	700	1	$La_{0.6}Sr_{0.4}CoO_{3-x}$, Co_3O_4, $SrCO_3$, unknown peaks at $d = 0.318$ and 0.326 nm	15
	900	1	$La_{0.6}Sr_{0.4}CoO_{3-x}$, $SrLaCoO_4$, Co_3O_4, unknown low intensity peaks at $d = 0.181$ and 0.351 nm	23
	1000	1	$La_{0.6}Sr_{0.4}CoO_{3-x}$, $SrLaCoO_4$, unknown very low intensity peaks at $d = 0.247$ and 0.354 nm	29
	1200	1	$La_{0.6}Sr_{0.4}CoO_{3-x}$	60
	1300	1	$La_{0.6}Sr_{0.4}CoO_{3-x}$	50
	1400	1	$La_{0.6}Sr_{0.4}CoO_{3-x}$	70
$Sm_{0.5}Sr_{0.5}CoO_{3-x}$	550	20	Co_3O_4, $SmCoO_3$, $SrCO_3$, unknown peak	
	700	1	$Sm_{0.5}Sr_{0.5}CoO_{3-x}$, $SrCO_3$, Co_3O_4, unknown peaks at $d = 0.317$ and 0.337 nm	15
	900	1	$Sm_{0.5}Sr_{0.5}CoO_{3-x}$, $Sr_3Co_2O_6$, Co_3O_4, unknown peaks at $d = 0.138$, 0.183, 0.305, and 0.357 nm	15
	1000	1	$Sm_{0.5}Sr_{0.5}CoO_{3-x}$, $Sr_3Co_2O_6$, Co_3O_4, same unknown peaks as at 900 °C	15
	1200	1	$Sm_{0.5}Sr_{0.5}CoO_{3-x}$, $Sr_3Co_2O_6$, unknown peak at $d = 0.158$ nm	27
	1300	1	$Sm_{0.5}Sr_{0.5}CoO_{3-x}$	100

[a] Phases in decreasing order of peak intensity.
[b] Calcualted from Scherrer formula using FWHM of XRD peak in 47–48° 2θ range.

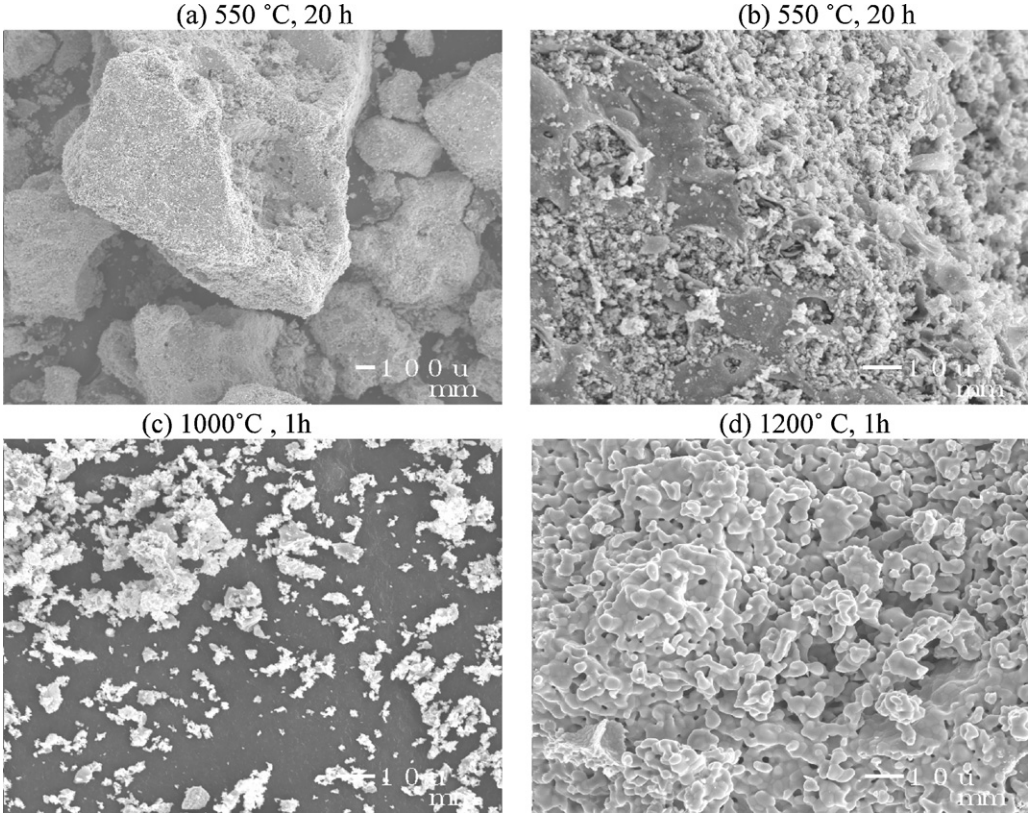

Fig. 5. SEM micrographs of $La_{0.6}Sr_{0.4}CoO_{3-x}$ sol–gel nanopowders calcined at various temperatures: (a and b) 550 °C, 20 h; (c) 1000 °C, 1 h; (d) 1200 °C, 1 h.

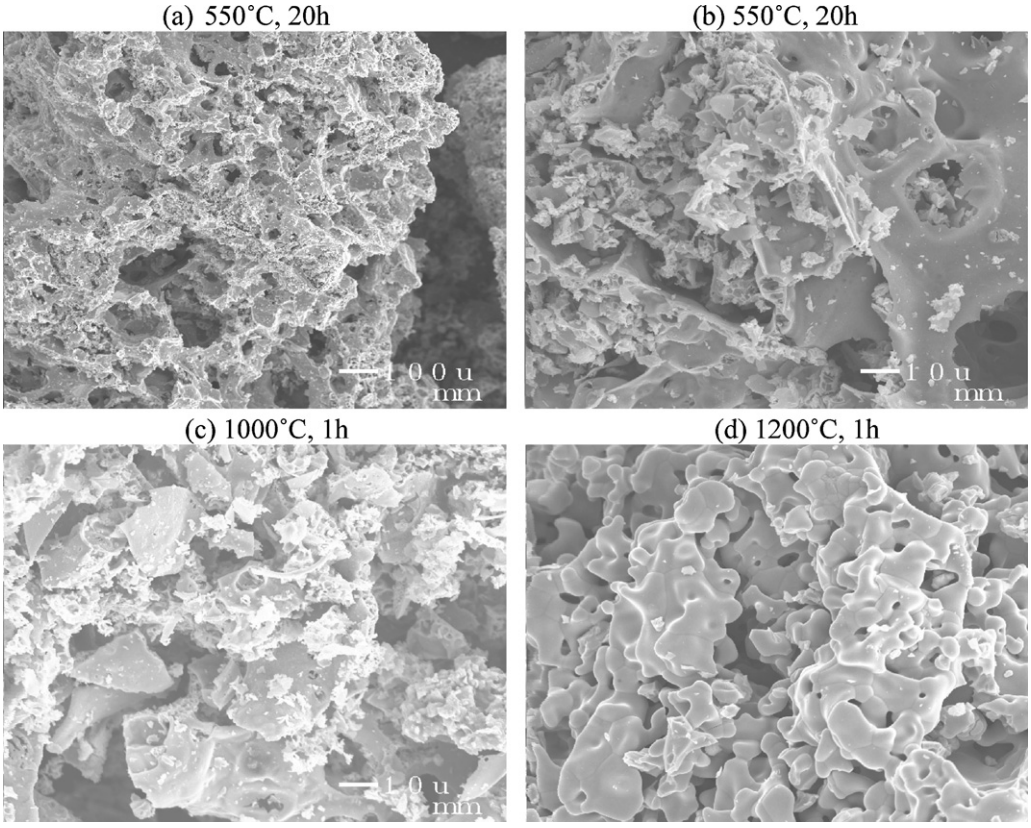

Fig. 6. SEM micrographs of $Sm_{0.5}Sr_{0.5}CoO_{3-x}$ sol–gel nanopowders calcined at various temperatures: (a and b) 550 °C, 20 h; (c) 1000 °C, 1 h; (d) 1200 °C, 1 h.

treatment at 550 °C were highly porous and quite small in size. The particle size increased with increase in heat treatment temperature. Heat treatment at 1200 °C resulted in large grain growth and densification of both the powders. It may also be noted that these values are much larger than those observed from XRD analysis. It is because the SEM measures only the particle size rather than the crystallite size and several crystallites may be present in a single particle in the SEM image.

The LSC and SSC nanopowders synthesized in this study will be used for cathode materials in the preparation of intermediate temperature solid oxide fuel cells (IT-SOFCs) with La(Sr)Ga(Mg)O_{3-x} (LSGM) as the electrolyte followed by their electrochemical characterization. The results of these SOFCs will be reported in the near future.

4. Summary and conclusions

Nano-powders of $La_{0.6}Sr_{0.4}CoO_{3-x}$ and $Sm_{0.5}Sr_{0.5}CoO_{3-x}$ compositions have been synthesized by low-temperature sol–gel process. Thermal decomposition of the gels was followed by simultaneous DSC/TGA methods. X-ray diffraction was used to follow the development of crystalline phases on heat treatments of the gel powders at various temperatures. Powders calcined at 550–1000 °C consisted of a number of phases. Powders containing single perovskite phase $La_{0.6}Sr_{0.4}CoO_{3-x}$ or $Sm_{0.5}Sr_{0.5}CoO_{3-x}$ were obtained at 1200 °C and 1300 °C, respectively. Morphological analysis of the powders calcined at various temperatures was done by scanning electron microscopy. The average crystallite size of the 700 °C calcined powders was ∼15 nm which slowly increased to 70–100 nm after heat treatments at 1300–1400 °C.

Acknowledgments

Thanks are due to John Setlock for DSC–TGA and to Ralph Garlick for X-ray diffraction analysis. This work was supported by NASA's Subsonic Fixed Wing Project of the Fundamental Aeronautics Program. Brent Wise was a co-op student from Case Western Reserve University at NASA Glenn Research Center during the time this work was carried out.

References

[1] N.Q. Minh, Ceramic fuel cells, Journal of the American Ceramic Society 76 (3) (1993) 563–588.

[2] F. Licci, G. Turilli, P. Ferro, A. Ciccarone, Low-temperature synthesis and properties of $LaMnO_{3\pm d}$ and $La_{0.67}R_{0.33}MnO_{3\pm d}$ (R = Ca, Sr, Ba) from citrate precursors, Journal of the American Ceramic Society 86 (3) (2003) 413–419.

[3] S. Uhlenbruck, F. Tietz, High temperature thermal expansion and conductivity of cobaltites: potentials for adaptation of the thermal expansion to the demands for SOFCs, Materials Science and Engineering B107 (3) (2004) 277–282.

[4] N.P. Bansal, Z. Zhong, Combustion synthesis of $Sm_{0.5}Sr_{0.5}CoO_{3-x}$ and $La_{0.6}Sr_{0.4}CoO_{3-x}$ nanopowders for solid oxide fuel cell cathodes, Journal of Power Sources 158 (1) (2006) 148–153.

[5] E. Djurado, M. Labeau, Second phases in doped lanthanum gallate perovskites, Journal of the European Ceramic Society 18 (1998) 1397–1404.
[6] R. Polini, A. Falsetti, E. Traversa, Sol-Gel Synthesis, Characterization of co-doped LSGM perovskites, Journal of the European Ceramic Society 25 (2005) 2593–2598.
[7] J. Wang, A. Manivannan, N. Wu, Sol–gel derived $La_{0.6}Sr_{0.4}CoO_{3-x}$ nanoparticles, nanotubes, nanowires and thin films, Thin Solid Films 517 (2) (2008) 582–587.
[8] B.D. Cullity, Elements of X-ray Diffraction, second ed., Addison-Wesley, Reading, MA, 1978, p. 284.